Localized electron dynamics in attosecond-pulse-excited molecular systems: Probing the time-dependent electron density by sudden photoionization

B. Mignolet,[1] R. D. Levine,[2] and F. Remacle[1,2,*]

[1]*Department of Chemistry, B6c, University of Liege, B4000 Liege, Belgium*

[2]*The Fritz Haber Research Center for molecular dynamics, The Hebrew University of Jerusalem, Jerusalem 91904, Israel*

(Received 16 August 2012; revised manuscript received 17 October 2012; published 30 November 2012)

Ultrafast UV excitation can prepare a nonstationary coherent superposition of molecular electronic states. The purely electronic dynamics before the onset of nuclear motion can be probed by a sudden XUV ionization of the electronic wave packet. Dynamical computations at the many-electron level on the LiH and 1-azabicyclo[3.3.3]undecane ($C_{10}H_{19}N$) molecules show that molecular frame photoelectron angular distributions reflect the spatial localization and undulations of the electronic coherent superposition accessed by the initial ultrafast UV excitation. The sudden ionization is sensitive to interference effects.

DOI: 10.1103/PhysRevA.86.053429 PACS number(s): 33.20.Xx, 33.60.+q, 33.80.−b

I. INTRODUCTION

Few-cycle photon pulses of a duration of a femtosecond and less enable exciting and probing electron dynamics in atoms and molecules in real time [1–7]. We are primarily interested in understanding the post-Born–Oppenheimer regime that spans the time scale of the purely electronic dynamics before the onset of the nuclear motion [8]. Characterizing that regime requires an ultrashort pulse also at the probe step. Such experiments have been recently reported for atoms [9] but remain an experimental challenge for molecular systems. Experimental setups are still limited to using one attosecond pulse only, either for the pump or for the probe step, the second pulse being a strong IR pulse with a typical duration of 10 fs or more during which the nuclei start to move. Typically, dissociation is then used to probe the electron-nuclei dynamics [7,10–13]. Often, an attosecond train pulse (ATP) is used [14–17], which can make the interpretation of the experimental results more complex.

To probe the localization and oscillation of the coherent electronic wave packet produced by an ultrashort excitation we use the molecular frame photoelectron angular distributions (MFPADs) [18,19]. The computation of photoionization rates and MFPADs for sudden ionization with an ultrashort strong XUV pulse follows the pump-probe scheme shown in Fig. 1. In order to probe the electronic dynamics as induced by the pump pulse it is desirable that the ionization process is as instantaneous as possible. Otherwise the probe pulse itself can perturb the electronic motion and it renders a blurred snapshot of the evolving state that is induced by the pump. The pump is an UV ultrashort pulse that prepares a coherent superposition of electronic states of the neutral molecule. This coherent superposition is then probed by a sudden XUV ionization. We show that the angular patterns of the computed MFPAD reflect the composition of the coherent electronic wave packet at the time of ionization and are sensitive to interference effects and their changes with time as the wave packet evolves.

*Corresponding author: fremacle@ulg.ac.be

II. PHOTOIONIZATION CROSS SECTION FOR THE SUDDEN IONIZATION

We use a scattering theoretic approach [20] and correlated many-electron wave functions for the neutral and the cation with nuclei frozen at the equilibrium geometry of the neutral. We consider the four-electron diatomic molecule LiH and a medium size rigid polyatomic molecule, 1-azabicyclo[3.3.3]undecane ($C_{10}H_{19}N$) (ABCU), with a nitrogen atom at the top of the cage and a total of 86 electrons; see Fig. 2. The caged polyatomic molecule ABCU has a richer potential of sites for localization of the electronic wave packet. We demonstrate that these too can be probed by sudden XUV ionization and interpreted using the patterns of the MFPAD.

The electronic structure of the ground state and excited states of LiH has been computed with the quantum chemistry suite of programs MOLPRO [21] using a complete active space–self-consistent field (CAS-SCF) average computation of 40 electronic states (15Σ, $10\Pi x$, $10\Pi y$, and 5Δ) with an active space of four electrons and 29 orbitals (13σ, $7\Pi x$, $7\Pi y$, and 2δ) and with the 6-311++$g(2df,2p)$ basis set [22]. The excitation spectrum is reported in Fig 2. The 15 lowest Σ excited states of the cation have been computed at the CAS-SCF level with the same active space and basis set and three active electrons. For both the neutral and the cation, the Li-H bond length is taken to be 1.63 Å and the computed ionization potential (IP) for the CAS-SCF average level is 7.67 eV. The equilibrium geometry of ABCU belongs to C_3 and has been optimized at the CAS-SCF level with an active space of eight electrons and 13 molecular orbitals and the 6-31++$G(d,p)$ basis set [23]. Its excitation spectrum is reported in Fig. 2. The same active space and basis were chosen to compute the electronic structure of the 18 lowest excited states and the ground state (GS) at the CAS-SCF average level. The ten lowest excited states of the cation have been computed at the geometry of the neutral in CAS average with seven active electrons and eight molecular orbitals and the same basis set. The computed IP at the CAS-SCF average level is 6.2 eV.

Each molecule has two sets of electronic states with different symmetry properties that can be excited from the ground state. Electronic states of A symmetry in ABCU are the analog of the Σ states in LiH and the doubly degenerate E ones the analogs of the LiH Π states. There is a significant transition

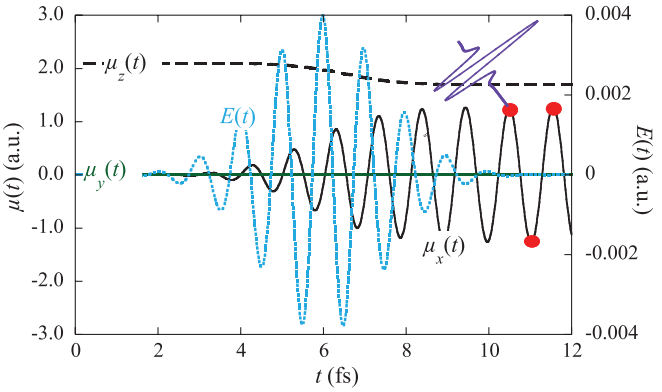

FIG. 1. (Color online) Scheme of the simulated pump-probe experiment for LiH. The pump excitation pulse, dotted curve, right ordinate, is polarized perpendicularly to the LiH bond (x direction; see Fig. 2) with a Gaussian envelope (centered at $t_0 = 250$ a.u., carrier frequency, $\omega_{\text{pump}} = 0.15$ a.u., with $\sigma = 60$ a.u., field strength, $E_0 = 0.004$ a.u.). XUV sudden ionization takes place at maximal intensity of the electric field, as indicated by the red dots, the delay between the pump and the probe pulse, $\tau = (t - t_0)$, is equal to 4.51, 5.04, and 5.57 fs. The time-dependent responses of the x and z components of the dipole are shown in full lines and dashes, respectively. μ_z does not oscillate since the pulse is polarized along x and its decrease reflects the depletion of the GS by the pump pulse. The oscillation of μ_x reflects the beatings of the coherent wave packet between the GS and the x component of the Π state.

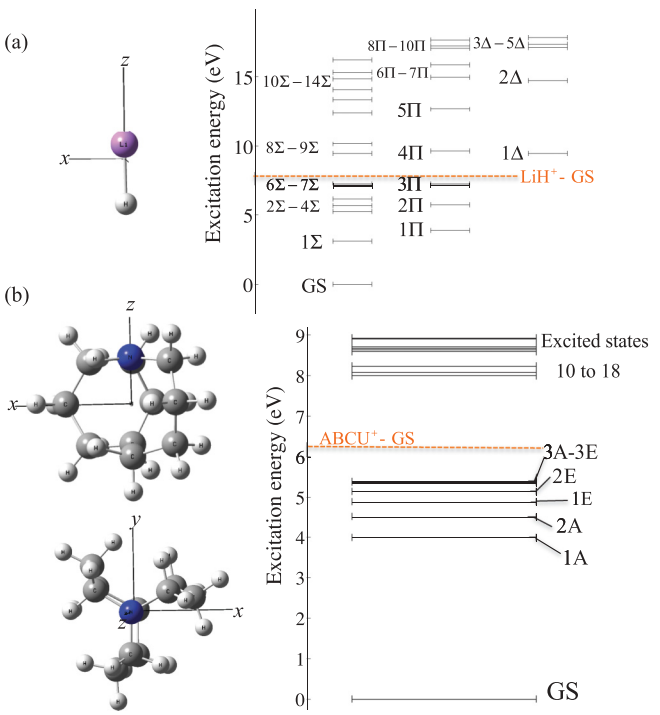

FIG. 2. (Color online) Equilibrium geometry and energy level diagram of the electronic states of LiH (a) and ABCU (b) computed at the equilibrium geometry of the GS at the CAS-SCF average level.

dipole moment from the ground state to both the singly and doubly degenerate excited states. Symmetry dictates that these transition dipoles are oriented along different directions in the molecular frame. Pure electronic wave-packet dynamics can be induced by ultrafast pumping to a superposition of excited states [22–25]. The ABCU molecule is quite rigid and LiH has a low vibrational frequency of ≈1300 cm^{-1} which provides a time window of about 10–15 fs before a significant motion of the nuclei takes place [22–25]. Moreover, their ground state exhibits a significant dipole moment along the molecular axis, $\mu_{\text{LiH}} = 2.08$ a.u. and $\mu_{\text{ABCU}} = -0.44$ a.u., which suggests that they could be oriented by a nonresonant laser field just before the electronic excitation [23,26,27]. In the case of ABCU, control of the orientation along the molecular axis is expected to be easier than controlling the orientation with respect to the three arms of the cage [23].

Various approaches have been proposed to solve the electron dynamics [22,23,25,28–35] and some include the coupling to the nuclei [33,36–40]. Attosecond pulses need to be intense in order to deliver enough energy so that a detectable number of ions is produced, which precludes the use of perturbative methods for computing the electron response both for the excitation and the ionization steps. To follow the electron dynamics, we solve the time-dependent Schrödinger equation for the time-dependent Hamiltonian that includes the interaction with the strong field in the basis of a large band of field-free many-electron states: in atomic units (a.u.) [22,23,41] $i d\mathbf{c}/dt = \mathbf{H}(t)\,\mathbf{c}$ with

$$H(t) = H^{\text{elec}} - \mathbf{E}\cdot\boldsymbol{\mu} f(t)\cos(\omega_{\text{pump}} t + \phi). \qquad (1)$$

In Eq. (1), H^{elec} is the field-free electronic Hamiltonian at the equilibrium geometry of the ground state. The interaction with the electric field, $\mathbf{E}$, is described in the dipole approximation, and $\boldsymbol{\mu}$ is the transition dipole of the molecule. ω_{pump} is the excitation frequency, ϕ the carrier envelope phase (CEP), and the field envelope is taken to be Gaussian, $f(t) = \exp[-(t - t_0)^2/2\sigma^2]$. The wave packet at time t is a coherent superposition of many-electron field-free states of the neutral, $|\Psi_I\rangle$, coupled by the transition dipole: $|\Psi(t)\rangle = \sum_I^N c_I(t)\,|\Psi_I\rangle$.

The photoionization cross section [Eq. (2) below] is sensitive to the characteristics of the coherent electronic wave packet at the time of ionization including interference effects. This is the central point of this paper: Sudden ionization of molecules can be used as an effective probe. Within the sudden approximation, photoionization is assumed to occur at the maximum of the electric field of the XUV probe pulse. In this case, the photoionization cross section of the electronic wave packet, $|\Psi(\tau)\rangle$ at time of ionization, $\tau = t - t_0$ (see Fig. 1), can be written in the Fermi Golden Rule approximation [42–45]:

$$\begin{aligned}\sigma_K(\varepsilon) &= \frac{4\pi\omega_{\text{probe}}}{\varepsilon_0 c E_0^2}\rho(\varepsilon)|\langle\Psi_{K,\varepsilon}|\mathbf{P}V\mathbf{Q}|\Psi(\tau)\rangle|^2 \\ &= \frac{4\pi\omega_{\text{probe}}}{\varepsilon_0 c}\rho(\varepsilon) \\ &\quad\times\left|\sum_I^N c_I(\tau)\langle\Psi_{K,\varepsilon}|\mathbf{P}\left(-e\frac{\mathbf{E}}{E_0}\sum_n \mathbf{r}_n\right)\mathbf{Q}|\Psi_I\rangle\right|^2. \qquad (2)\end{aligned}$$

In Eq. (2), $\mathbf{Q}$ and $\mathbf{P}$ are the complementary projectors on the bound and continuous subspaces. E_0 is the maximum amplitude of the electric field, ω_{probe} the carrier frequency of the ionizing pulse, c the speed of light, and $\rho(\varepsilon)$ is the density

of the continuum states at the kinetic energy ε of the ionized electron in the channel K. $V = -e\mathbf{E}\sum_n \mathbf{r}_n$ is the dipole coupling between the field-free n electron bound states of the neutral molecule, $|\Psi_I\rangle$, and the states of the continuum, $|\Psi_{K,\varepsilon}\rangle$, defined as the antisymmetrized product of the $n-1$ electron eigenstates of the cation and a plane wave. This approximation assumes that a single electron is active and neglects the Coulomb and exchange interactions between the departing electron and the remaining $n-1$ electrons cation. It is justified for a one-photon XUV sudden ionization which we consider here. However, electrostatic and exchange interactions play an important role in multiphoton IR ionization [45–47]. An estimate of the relative importance of tunnel and multiphoton ionization with respect to one-photon ionization is given by the value of the Keldysh parameter, γ [2]. For XUV ionizing ultrashort pulses, with a carrier wavelength of the order of 10–15 eV, and an electric field strength of the order of 0.03 a.u., γ is of the order of 5–15. In that regime where $\gamma \gg 1$, tunnel ionization can be neglected as well as multiphoton absorption. Electron-electron interactions also play a role in autoionization. Autoionization is a slower process induced by the multipolar interactions between the cation and the leaving electron which typically occurs in the nanosecond regime [48,49]. This process is not expected to contribute significantly in the ultrashort time scale of interest here. We also neglect indirect autoionization following an Auger process [9,50].

The states of the continuum are orthogonalized to those of the bound states to ensure that $\mathbf{PQ} = 0$. $\mathbf{Q} = \sum |\Psi_I\rangle\langle\Psi_I|$ and $\mathbf{P} = \sum_K \int d\varepsilon_K |\Psi_K^{\rm cat},\varepsilon_K^\perp\rangle\langle\Psi_K^{\rm cat},\varepsilon_K^\perp|$ where $|\Psi_K^{\rm cat}\rangle$ is the Kth $n-1$ electron field free state of the cation and $|\varepsilon_K^\perp\rangle$ is the wave function of the electron for channel K. It is approximated as a plane wave orthogonalized to the molecular orbitals (MOs) of the neutral: $|\varepsilon_K^\perp\rangle = |\varepsilon_K\rangle - \sum_{i=1}^m \langle\phi_i^{\rm neut}|\varepsilon_K\rangle|\phi_i^{\rm neut}\rangle$ [42–44]. The $|\phi_i^{\rm neut}\rangle$ are the m average CAS-SCF MOs of the neutral and the plane waves, $|\varepsilon_K\rangle$, normalized on a box of dimension L :$|\varepsilon_K\rangle = \exp(i\mathbf{k}\cdot\mathbf{r})/L^{3/2}$ with $\varepsilon = k^2/2m$. The states of the continuum subspace $\mathbf{P}$ are given as the antisymmetrized product of the antisymmetrized wave function of the cation and that of the free electron:

$$|\Psi_K^{\rm cat},\varepsilon_K^\perp\rangle = \frac{1}{\sqrt{2}}\frac{1}{\sqrt{n}}\left(1-\sum_{j=1}^{n-1}\hat{P}_{jn}\right) \times\left[|\Psi_K^{\rm cat}(\alpha)\varepsilon_K^\perp(\beta)\rangle - |\Psi_K^{\rm cat}(\beta)\varepsilon_K^\perp(\alpha)\rangle\right]$$

where $\hat{P}_{jn}$ is the operator that interchanges the coordinate of electron j of the cation with those of electron n of the plane wave. Taking into account that the spatial part of the wave function of the cation and free electron is the same for the spin α and β and the indistinguishability of electrons, the wave function can be rewritten as $|\Psi_K^{\rm cat},\varepsilon_K^\perp\rangle = \sqrt{2}\sqrt{n}|\Psi_K^{\rm cat}(\beta)\varepsilon_K^\perp(\alpha)\rangle$. The working expression of bound continuum matrix elements that appear in the expression of the photoionization cross section [Eq. (2)] takes antisymmetrization into account and is given by

$$\langle\Psi_K^{\rm cat},\varepsilon_K^\perp|V|\Psi_I\rangle = -e\mathbf{E}\sqrt{2}\left[\langle\phi_{IK}^D|\mathbf{r}|\varepsilon_K\rangle - \sum_i^m \langle\phi_{IK}^D|\mathbf{r}|\phi_i^{\rm neut}\rangle\langle\phi_i^{\rm neut}|\varepsilon_K\rangle\right]. \quad (3)$$

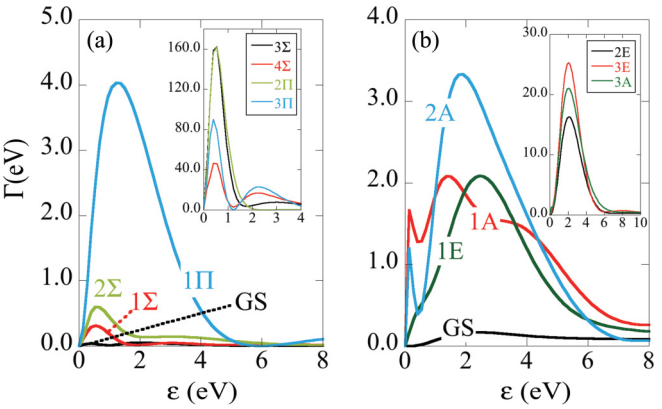

FIG. 3. (Color online) The computed photoionization rates (in eV) of the GS and lowest excited state of LiH (a) and ABCU (b), as a function of the kinetic energy, ε, of the ionized electron for a pulse polarized in the z direction with a maximum amplitude $E_0 = 0.05$ a.u. The ionization rates of the higher excited states are shown in the insets. They are comparable for the two molecules but those of ABCU decrease slower as a function of ε than those of LiH. The variation with ε close to the IP suggests that threshold effects play an important role for IR multiphoton ionization.

The Dyson orbitals [42,51,52], $\phi_{IK}^D = \sqrt{n}\int \Psi_K^{\rm cat}\Psi_I dr_1\cdots dr_{n-1}$, can be expanded in the MOs of the neutral to get $|\phi_{IK}^D\rangle = \sum_{i=1}^m c_{IK,i}^D|\phi_i^{\rm neut}\rangle$. They represent the density amplitude of an electron ionizing from state I into channel K. Their densities are shown in Figs. 4 and 5 below. Up to the orthogonalization factor, the photoionization amplitude of Eq. (3) is the Fourier transform of the dipole moment of Dyson orbital to momentum space. Two additional phase shifts may arise: first, when the interaction of the departing electron with the $n-1$ electrons that remain bound is taken into account. The remaining electrons are, however, localized and there is little time for the departing electron to collect a substantial phase shift in this way. A second phase shift arises when it is necessary to go beyond the sudden photoionization approximation and include the additional electron dynamics that is induced by the probe process. The dipole moment of the Dyson orbital is also used in tomography of orbitals by high harmonic generation [4,53,54].

The photoionization widths, $\Gamma(\varepsilon) = \rho(\varepsilon)|\langle\Psi_K^{\rm cat},\varepsilon_K^\perp|V|\Psi_I\rangle|^2$, vary with the kinetic energy, ε, above the ionization threshold. Those of the lowest electronic states of the neutral LiH and ABCU molecules are shown in Fig. 3. The photoionization lifetimes are reported in Tables I and II for $\varepsilon = 1.0$ and 6.0 eV above the ionization threshold (IP). As can be expected from Eq. (3), the more diffuse high Σ and Π states of LiH and the high A and E states of ABCU have

TABLE I. Lifetimes of the lowest excited states of LiH for $E_0 = 0.05$ a.u., polarized along z.

	Lifetimes in fs						
	GS	1Σ	2Σ	3Σ	4Σ	1Π	2Π
$\varepsilon = 1.0$ eV	57.4	3.2	1.4	0.01	0.06	0.2	0.01
$\varepsilon = 6.0$ eV	123.1	33.1	14.8	0.8	0.3	480	3.9

TABLE II. Lifetimes of the lowest excited states of ABCU for $E_0 = 0.05$ a.u. polarized along z.

	Lifetimes in fs			
	GS	1A	1E	2A
$\varepsilon = 1.0$ eV	10.7	0.4	0.8	0.7
$\varepsilon = 6.0$ eV	7.1	1.1	2.0	1.9

larger ionization rates, by two orders of magnitude or more, than the GS, with lifetimes in the attosecond to femtosecond range for kinetic energies close to the IP. If these states are accessed by multiphoton processes during the pump pulse, they will ionize and the bound state dynamics will be affected. For this reason, in the results reported below, we use pump pulse intensities small enough to avoid significant population of these higher excited states. For the higher electron kinetic energies typical of XUV ionization (6–8 eV), the lifetimes of the low excited states vary smoothly with energy and are of the order of several to dozens of femtoseconds, an order of magnitude or longer than close to the ionization threshold.

The angular resolved cross section in the solid angle $d\Omega$ takes the form

$$\frac{d\sigma_K(\varepsilon)}{d\Omega} = \frac{8\pi e^2 \omega_{\text{probe}}}{\varepsilon_0 c}\rho_\Omega(\varepsilon)\left|\sum_I c_I(\tau)\left(\frac{\mathbf{E}}{E_0}\langle\phi^D_{IK}|\mathbf{r}|\varepsilon_{K,\Omega}\rangle - \sum_i^m \frac{\mathbf{E}}{E_0}\langle\phi^D_{IK}|\mathbf{r}|\phi_i^{\text{neut}}\rangle\langle\phi_i^{\text{neut}}|\varepsilon_{K,\Omega}\rangle\right)\right|^2. \quad (4)$$

As can be seen from Eq. (4), the MFPAD pattern of a specific excited state, $|\Psi_I\rangle$, will be dictated by the spatial extension of the corresponding Dyson orbital. The Dyson orbitals and the corresponding MFPAD calculated for an electron kinetic energy 6.0 eV above the IP are shown in Fig. 4

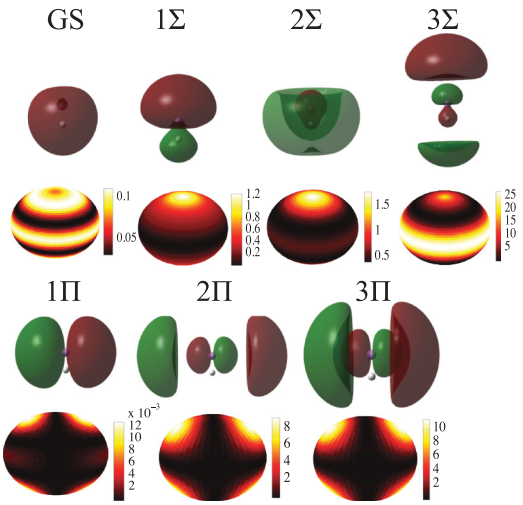

FIG. 4. (Color online) Dyson orbitals (top) and MFPAD (bottom) of the lowest excited states of LiH. The photoionization cross sections (expressed in $1.15\omega_{\text{probe}}$ bohr^2, where ω_{probe} is the frequency of the XUV pulse) are computed for a kinetic energy, $\varepsilon = 6.0$ eV, and for a polarization of the XUV pulse along z.

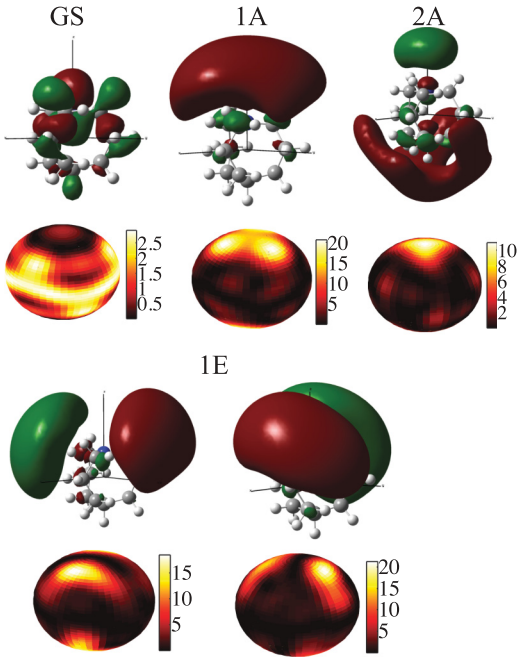

FIG. 5. (Color online) Dyson orbitals (top) and MFPAD (bottom) of the lowest A and E (doubly degenerate) excited states of ABCU. The MFPAD (expressed in $1.15\omega_{\text{probe}}$ bohr^2, where ω_{probe} is the frequency of the XUV pulse) are computed for a kinetic energy, $\varepsilon = 6.8$ eV, and for a polarization of the XUV pulse along z.

for the GS and the lowest excited states of LiH and in Fig. 5 for ABCU.

III. RESULTS AND DISCUSSION

A. Diatomic molecule: LiH

The excitation of the lowest Π state in LiH by a pump pulse polarized in the x direction is shown in Fig. 1. The pump pulse is chosen to be weak ($E_0 = 0.004$ a.u.) so that the excitation is a one-photon transition to the $1\Pi_x$ state with essentially no population in higher states and no ionization occurring during the pump pulse. At the end of the pulse, a superposition of the GS (82%) and of $1\Pi_x$ (18%) is built. Fig. 6(a) shows isocontours of their stationary electronic densities as well as of the transition density, $\rho_{\text{GS}-\Pi_x}(r) = n\int \Psi^*_{\text{GS}}(r_1, r_2 \cdots r_n)\,\Psi_{\Pi_x}(r_1, r_2 \cdots r_n)dr_2 \cdots dr_n$ that reflects the change of electronic density in the transition between the GS and Π_x state [55]. The electron density, $\rho(\tau)$, that corresponds to the superposition of states, is shown in Fig 6(b). It beats along the x direction with a period of 1.06 fs, reflecting the relatively large energy difference between the GS and the excited Π state. The spatial localization of the beatings reflects the shape of the transition matrix, $\rho_{\text{GS}-\Pi_x}$.

For the simple case when a superposition of two states is built at the end of the pulse, the photoionization cross section, Eq. (2), computed at a delay time, τ, between the pump and the probe XUV pulse (see Fig. 1), takes the form

$$\sigma(E) \propto |c_{\text{GS}}|^2|\langle\Psi^{+\perp}_{K,\varepsilon}|V|\Psi_{\text{GS}}\rangle|^2 + |c_{1\Pi x}|^2\left|\langle\Psi^{+\perp}_{K,\varepsilon}|V|\Psi_{1\Pi x}\rangle\right|^2 + 2\cos[(E_{\text{GS}} - E_{1\Pi_x})\tau]\langle\Psi^{+\perp}_{K,\varepsilon}|V|\Psi_{\text{GS}}\rangle \times \langle\Psi_{1\Pi x}|V|\Psi^{+\perp}_{K,\varepsilon}\rangle. \quad (5)$$

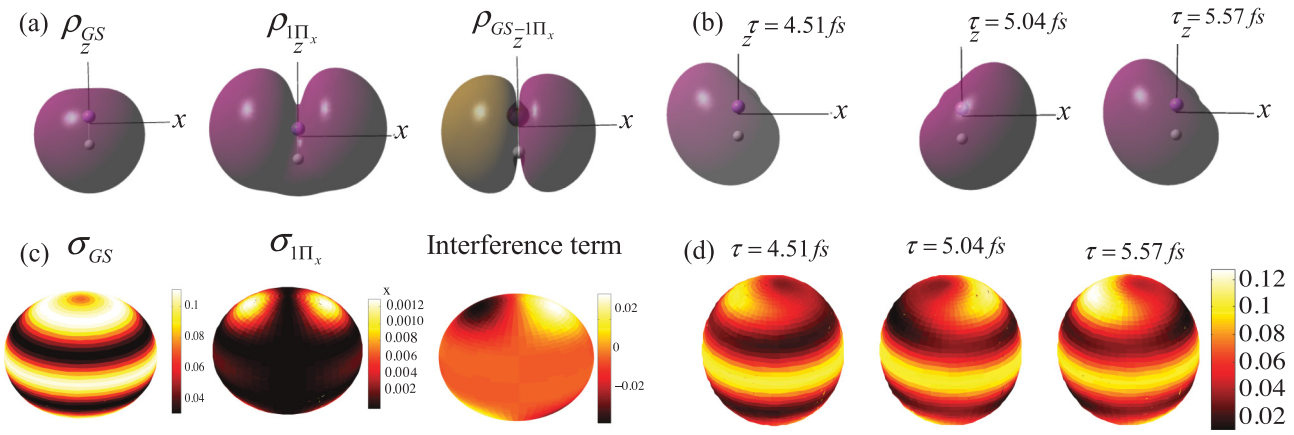

FIG. 6. (Color online) (a) Stationary electronic densities, ρ, of the GS and the $1\Pi_x$ state and transition density between the GS and $1\Pi_x$ state computed for an isocontour value of $0.0001|e|/\text{Å}^3$. (b) $\rho(\tau)$ computed for the coherent superposition of states built by the pump pulse of Fig. 1 and pump-probe delays τ of 4.51, 5.04, and 5.57 fs shown as red dots therein. (c) MFPAD, Eq. (4), (in 0.55 bohr^2) of the GS and of the $1\Pi x$ state and the cross term computed for a XUV pulse ($\omega_{\text{probe}} = 13.0$ eV and $\varepsilon = 6.0$ eV) polarized along z. (d) MFPAD computed for $|\Psi(\tau)\rangle$ in Eq. (4) with $\tau = 4.51$, 5.04, and 5.57 fs and the same XUV pulse.

When the pump pulse is over, the Hamiltonian is time independent and the system is stationary until sudden ionization by the probe pulse. Its energy is given by $E_\Psi = \langle\Psi(t)|\, H^{\text{elec}}\, |\Psi(t)\rangle$ with $|\Psi(t)\rangle = c_{\text{GS}}(t)\,|\Psi_{\text{GS}}\rangle + c_{1\Pi}(t)\,|\Psi_{1\Pi}\rangle$. Both stationary states ionize to the GS of the cation and the kinetic energy of the electron ε is given by $\varepsilon = E_\Psi + \hbar\omega_{\text{probe}} - E^{\text{cat}}_{\text{GS}}$. The MFPADs of the GS and of the Π state are shown separately in Fig. 6(c) as well as the interference term, which corresponds to $\langle\Psi^{+\perp}_{K,\varepsilon}|V|\Psi_{\text{GS}}\rangle\langle\Psi_{1\Pi x}|V|\Psi^{+\perp}_{K,\varepsilon}\rangle$ in the second line of Eq. (5). They are computed for a sudden ionization by an XUV ($\omega_{\text{probe}} = 13.0$ eV) pulse polarized in the z direction, which leads to a kinetic energy, ε, of 6.0 eV for the leaving electron. For this value of ε, the total photoionization widths, Γ, are comparable (see Fig. 3 and Table I), and of the order of 0.004 eV. One can see from Fig. 6(c) that the interference term in Eq. (5) removes ionization amplitude from the positive and negative x direction alternatively. The MFPAD [Eq. (4)] computed at different delay times τ are modulated by the interference term and are seen to reflect the oscillations of the electron density along the x direction; see Fig. 6(d). Figure 7 shows the integrated yield of ionization along the positive and negative x directions.

To induce a rotational motion of the electronic density in the (x,y) plane instead of a simple beating, one needs to pump the molecule with circularly polarized light with a phase difference of $\pi/2$ between the x and y components. The resulting MFPADs are shown in Fig. 8.

B. Polyatomic molecule: ABCU

Next we discuss electronic dynamics and its probing in the cage, $C_{10}H_{19}N$ (ABCU), molecule. The pump pulse is optimized to build a coherent electronic state that is a superposition of the GS (68%) and of two low excited states, the second A (2A) (18%) and one of the components of the first E (1E) state (10%). The densities of these three states are shown in Fig. 9(a). The GS and the $2A$ states have permanent dipole moments of opposite direction along z, while that of the $1E$ state is oriented at $-45°$ in the (x,y) plane. Consequently, the fast beatings of the electronic density, $\rho(t)$, are a superposition of the beating between the GS and the $2A$ state, that takes place along the z direction and that between the GS and the $1E$ state which occurs at 45° in the (x,y) plane. The period is of the order of 1 fs, since it is governed by the energy difference between the GS and the low excited states. It is comparable to that shown in Fig. 6 for LiH. Spatially, because it involves the GS, the motion of the electron density is localized close to the carbon cage, as can be seen from the isocontours of the transition matrices $\rho_{\text{GS}-2A}$, $\rho_{\text{GS}-1E}$, and ρ_{2A-1E} shown in the bottom row of panel (a) of Fig. 9.

On the other hand, there is a much slower beating period of $\rho(t)$ equal to 11.28 fs, that is governed by the energy difference between the two excited states, $\Delta E_{A-E} = 0.36$ eV. The two

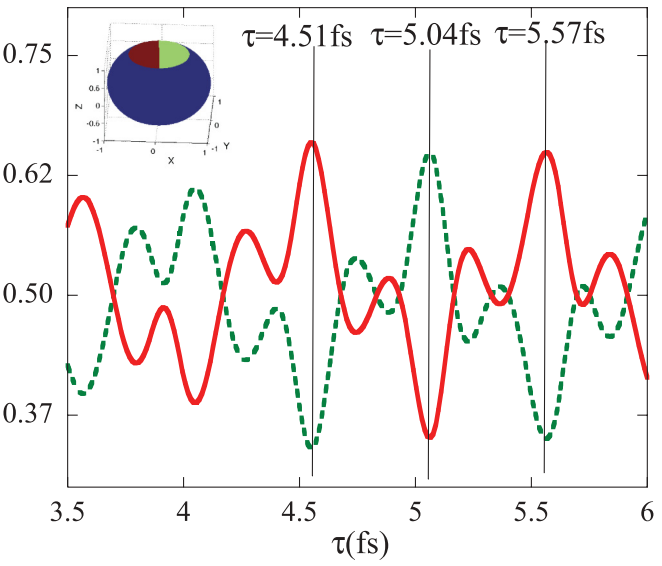

FIG. 7. (Color online) Fractional ionization yield, $y_{+X} = \frac{Y_{+X}}{Y_{+X}+Y_{-X}}$, computed for the $+x$ (dotted green line) and the $-x$ (red solid line) directions by integration of the differential cross section shown in Fig. 6(d)) on the solid angle shown in the inset.

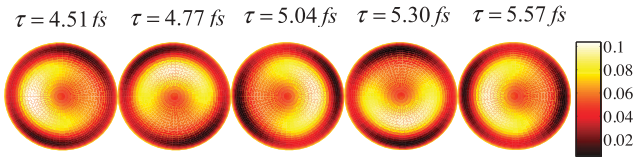

FIG. 8. (Color online) x-y view of the photoionization cross section computed for a pump-probe delay, τ, of 4.51, 4.77, 5.04, 5.30, and 5.57 fs (in 0.55 bohr^2). The pump pulse is polarized in the x-y plane in order to access the $1\Pi_x$ and $1\Pi_y$ components and induce a rotation motion in that plane. The pump pulse parameters are $t_0 = 250$ a.u., $\sigma = 60$ a.u., $\omega = 0.15$ a.u. with a carrier envelope dephasing of 90° between the x and y components; E_0 along the x and the y directions is $0.004/\sqrt{2}$ a.u. The XUV probe pulse ($\omega_{\text{probe}} = 13.0$ eV, $\varepsilon = 6.0$ eV) is polarized along z. The MFPAD patterns clearly exhibit a rotation in the (x,y) plane, whose period is dictated by the energy difference between the GS and the Π excited state.

beating periods of $\rho(t)$ are reflected in the oscillations of the mean value of the dipole moment along x and the z directions shown in Fig. 9(c). The slow beatings of $\rho(t)$ are shown in Fig 9(d). The interesting point is that spatially, because the excited states are more diffuse than the ground state, the electronic motion that corresponds to the slow beating period induced by the transition matrix, ρ_{2A-1E} [see Fig. 9(a)], occurs far from the cage.

The slow beatings in the MFPAD shown in Fig. 9(e) reflect the slower beating of the electronic density due to the interference between the two excited states. At $\varepsilon = 6.8$ eV, the $2A$ and $1E$ states have comparable ionization lifetimes (Table II). As can be seen from the MFPAD shown in Fig. 9(b), the $2A$ state ionizes preferentially from the top of the cage, while the $1E$ state presents maxima at 45% in the (x,y) plane. The interference term $\langle\Psi^{+\perp}_{K,\varepsilon}|V|\Psi_{2A}\rangle\langle\Psi_{1E}|V|\Psi^{+\perp}_{K,\varepsilon}\rangle$ [see Eq. (5)], changes sign along this direction. At $\tau = 5.98$ fs, the interference term between the two excited states is minimum, which corresponds to preferential ionization in the $(+x,-y)$ quadrant; see Fig. 9(e). When the interference term is maximum, at $\tau = 11.38$ fs, the maximum of ionization is obtained in the $(-x,+y)$ quadrant. When the interference term is close to zero, at $\tau = 8.5$ fs, the maximum of ionization is along the $-45°$ in the (x,y) plane .

IV. CONCLUSION

In conclusion, we showed computationally that the MFPADs computed for a sudden XUV ionization are a suitable probe of the coherent purely electronic motion initiated by a few-femtosecond UV pump pulse. The MFPADs reflect the spatial localization of the Dyson orbitals of the electronic states present in the coherent superposition built at the end of the pump pulse and therefore reflect the beatings of the electron density. In particular, the complex motion corresponding to

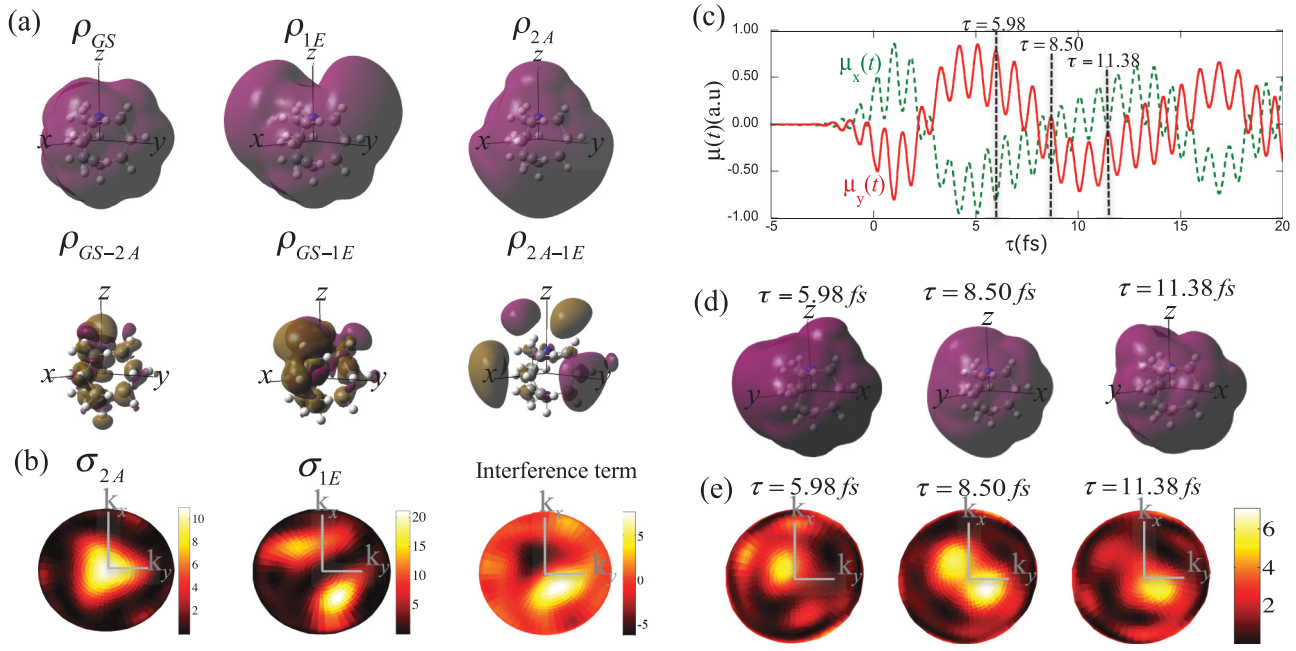

FIG. 9. (Color online) (a) Electronic densities of the GS, second A, lowest E states and transition density matrices $\rho_{\text{GS-1}E}$, $\rho_{\text{GS-2}A}$, and $\rho_{2A\text{-}1E}$ between the three electronic states taking part in the coherent superposition of states at the end of the pulse. Computed for an isocontour value of 0.0002$|e|$/Å^3. (b) x-y view of the MFPAD (in 0.29 bohr^2), Eq. (4), of the $2A$ and $1E$ states and their interference term computed for an XUV pulse ($\omega_{\text{probe}} = 11.7$ eV and $\varepsilon = 6.8$ eV) polarized along z. (c) Time-dependent responses of the x and y components of the dipole moment, $\mu_x(t)$ and $\mu_y(t)$, for an excitation by a short pump UV pulse ($t_0 = 250$ a.u., $\omega_{\text{pump}} = 0.179$ a.u., $\sigma = 50$ a.u., $E_0 = 0.03$ a.u. with components $E_x = 0.223$, $E_y = -0.223$, $E_z = 0.95$). The two components clearly exhibit the two time scales associated with the GS-1E and GS-2A energy differences (fast beating of ≈1 fs) and the $1E$-$2A$ energy difference (slow beating of 11.28 fs). (d) $\rho(\tau)$ computed for coherent superposition of state built by the pump pulse at a pump-probe delay of 5.98, 8.50, and 11.38 fs. (e) MFPAD computed for $|\Psi(\tau)\rangle$ [Eq. (4)] at $\tau = 5.98$, 8.50, and 11.38 fs.

a coherent superposition of several states can be analyzed in the polyatomic molecule ABCU, because of the different time scales and spatial localizations of the electronic states involved. Beatings between excited states close in energy are slower and correspond to an electronic motion of the electronic density that occurs far from the carbon cage because the excited electronic states are more diffuse.

ACKNOWLEDGMENTS

F.R. and B.M. acknowledge support from the Fonds de la Recherche Fondamentale Collective FRFC.2.4545.12 and support from the Fonds National de la Recherche Scientifique (FNRS, Belgium). Support by the Einstein Foundation of Berlin is gratefully acknowledged.

[1] P. B. Corkum and F. Krausz, Nat. Phys. **3**, 381 (2007).
[2] M. F. Kling and M. J. J. Vrakking, Annu. Rev. Phys. Chem. **59**, 463 (2008).
[3] F. Krausz and M. Ivanov, Rev. Mod. Phys. **81**, 163 (2009).
[4] O. Smirnova, Y. Mairesse, S. Patchkovskii, N. Dudovich, D. Villeneuve, P. Corkum, and M. Y. Ivanov, Nature **460**, 972 (2009).
[5] Y. Huismans *et al.*, Science **331**, 61 (2011).
[6] L. Gallmann, C. Cirelli, and U. Keller, Annu. Rev. Phys. Chem. **63**, 447 (2012).
[7] X. Zhou, P. Ranitovic, C. W. Hogle, J. H. D. Eland, H. C. Kapteyn, and M. M. Murnane, Nat. Phys. **8**, 232 (2012).
[8] F. Remacle and R. D. Levine, Proc. Natl. Acad. Sci. USA **103**, 6793 (2006).
[9] E. Goulielmakis, Z.-H. Loh, A. Wirth, R. Santra, N. Rohringer, V. S. Yakovlev, S. Zherebtsov, T. Pfeifer, A. M. Azzeer, M. F. Kling, S. R. Leone, and F. Krausz, Nature **466**, 739 (2010).
[10] M. F. Kling *et al.*, Science **312**, 246 (2006).
[11] F. Kelkensberg, C. Lefebvre, W. Siu, O. Ghafur, T. T. Nguyen-Dang, O. Atabek, A. Keller, V. Serov, P. Johnsson, M. Swoboda, T. Remetter, A. L'Huillier, S. Zherebtsov, G. Sansone, E. Benedetti, F. Ferrari, M. Nisoli, F. Lépine, M. F. Kling, and M. J. J. Vrakking, Phys. Rev. Lett. **103**, 123005 (2009).
[12] G. Sansone, F. Kelkensberg, J. F. Pérez-Torres, F. Morales, M. F. Kling, W. Siu, O. Ghafur, P. Johnsson, M. Swoboda, E. Benedetti, F. Ferrari, F. Lépine, J. L. Sanz-Vicario, S. Zherebtsov, I. Znakovskaya, A. L'Huillier, M. Yu. Ivanov, M. Nisoli, F. Martín, and M. J. J. Vrakking, Nature **465**, 763 (2010).
[13] P. Wernet, Phys. Chem. Chem. Phys. **13**, 16941 (2011).
[14] J. Mauritsson, P. Johnsson, E. Gustafsson, A. L'Huillier, K. J. Schafer, and M. B. Gaarde, Phys. Rev. Lett. **97**, 013001 (2006).
[15] N. Dudovich, O. Smirnova, J. Levesque, Y. Mairesse, M. Y. Ivanov, D. M. Villeneuve, and P. B. Corkum, Nat. Phys. **2**, 781 (2006).
[16] K. P. Singh, F. He, P. Ranitovic, W. Cao, S. De, D. Ray, S. Chen, U. Thumm, A. Becker, M. M. Murnane, H. C. Kapteyn, I. V. Litvinyuk, and C. L. Cocke, Phys. Rev. Lett. **104**, 023001 (2010).
[17] W. Li, A. A. Jaron-Becker, C. W. Hogle, V. Sharma, X. Zhou, A. Becker, H. C. Kapteyn, and M. M. Murnane, Proc. Natl. Acad. Sci. USA **107**, 20219 (2010).
[18] D. M. Neumark, Annu. Rev. Phys. Chem. **52**, 255 (2001).
[19] A. Stolow and J. G. Underwood, in *Advances in Chemical Physics*, edited by S. A. Rice (John Wiley & Sons Inc., New York, 2008), Vol. 139, p. 497.
[20] R. D. Levine, *Quantum Mechanics of Molecular Rate Processes* (Dover, Mineola, NY 1999).
[21] H.-J. Werner *et al.*, *MOLPRO: A Package of Ab Initio Programs*, Cardiff, UK, 2009.
[22] F. Remacle and R. D. Levine, Phys. Rev. A **83**, 013411 (2011).
[23] B. Mignolet, A. Gijsbertsen, M. J. J. Vrakking, R. D. Levine, and F. Remacle, Phys. Chem. Chem. Phys. **13**, 8331 (2011).
[24] F. Remacle, R. Kienberger, F. Krausz, and R. D. Levine, Chem. Phys. **338**, 342 (2007).
[25] F. Remacle, M. Nest, and R. D. Levine, Phys. Rev. Lett. **99**, 183902 (2007).
[26] O. Ghafur, A. Rouzee, A. Gijsbertsen, W. K. Siu, S. Stolte, and M. J. J. Vrakking, Nat. Phys. **5**, 289 (2009).
[27] L. Holmegaard, J. H. Nielsen, I. Nevo, H. Stapelfeldt, F. Filsinger, J. Kupper, and G. Meijer, Phys. Rev. Lett. **102**, 023001 (2009).
[28] J. Caillat, J. Zanghellini, M. Kitzler, O. Koch, W. Kreuzer, and A. Scrinzi, Phys. Rev. A **71**, 012712 (2005).
[29] A. D. Bandrauk, S. Chelkowski, and H. S. Nguyen, Int. J. Quantum Chem. **100**, 834 (2004).
[30] H. Hennig, J. Breidbach, and L. S. Cederbaum, J. Phys. Chem. A **109**, 409 (2005).
[31] I. Barth and J. Manz, Phys. Rev. A **75**, 012510 (2007).
[32] T. Kato and H. Kono, Chem. Phys. **366**, 46 (2009).
[33] H. Kono, Y. Sato, N. Tanak, T. Kato, K. Nakai, S. Koseki, and Y. Fujimura, Chem. Phys. **304**, 203 (2004).
[34] T. T. Nguyen-Dang, M. Peters, S.-M. Wang, E. Sinelnikov, and F. Dion, J. Chem. Phys. **127**, 174107 (2007).
[35] A. I. Kuleff and L. S. Cederbaum, Phys. Rev. Lett. **106**, 053001 (2011).
[36] A. D. Bandrauk, S. Chelkowski, S. Kawai, and H. Z. Lu, Phys. Rev. Lett. **101**, 153901 (2008).
[37] B. H. Muskatel, F. Remacle, and R. D. Levine, Phys. Scr. **80**, 048101 (2009).
[38] I. S. Ulusoy and M. Nest, J. Chem. Phys. **136**, 054112 (2012).
[39] P. von den Hoff, R. Siemering, M. Kowalewski, and R. de Vivie-Riedle, IEEE J. Sel. Top. Quantum Electron. **18**, 119 (2012).
[40] H. Mineo, M. Kanno, H. Kono, S. D. Chao, S. H. Lin, and Y. Fujimura, Chem. Phys. **392**, 136 (2012).
[41] G. Periyasamy, R. D. Levine, and F. Remacle, Chem. Phys. **366**, 129 (2009).
[42] G. M. Seabra, I. G. Kaplan, V. G. Zakrzewski, and J. V. Ortiz, J. Chem. Phys. **121**, 4143 (2004).
[43] F. O. Ellison, J. Chem. Phys. **61**, 507 (1974).
[44] M. Deleuze, B. T. Pickup, and J. Delhalle, Mol. Phys. **83**, 655 (1994).
[45] L. L. Lohr and M. B. Robin, J. Am. Chem. Soc. **92**, 7241 (1970).
[46] F. H. M. Faisal and G. Schlegel, J. Phys. B **38**, L223 (2005).
[47] O. Smirnova, M. Spanner, and M. Ivanov, Phys. Rev. A **77**, 033407 (2008).
[48] U. Fano, Phys. Rev. **124**, 1866 (1961).
[49] J. L. Sanz-Vicario, H. Bachau, and F. Martín, Phys. Rev. A **73**, 033410 (2006).

[50] M. Uiberacker, T. Uphues, M. Schultze, A. J. Verhoef, V. Yakovlev, M. F. Kling, J. Rauschenberger, N. M. Kabachnik, H. Schröeder, M. Lezius, K. L. Kompa, H.-G. Muller, M. J. J. Vrakking, S. Hendel, U. Kleineberg, U. Heinzmann, M. Drescher, and F. Krausz, Nature **446**, 627 (2007).

[51] B. T. Pickup, Chem. Phys. **19**, 193 (1977).

[52] C. M. Oana and A. I. Krylov, J. Chem. Phys. **127**, 234106 (2007).

[53] J. Itatani, J. Levesque, D. Zeidler, H. Niikura, H. Pepin, J. C. Kieffer, P. B. Corkum, and D. M. Villeneuve, Nature **432**, 867 (2004).

[54] S. Haessler, J. Caillat, W. Boutu, C. Giovanetti-Teixeira, T. Ruchon, T. Auguste, Z. Diveki, P. Breger, A. Maquet, B. Carré, R. Taïeb, and P. Salières, Nat. Phys. **6**, 200 (2010).

[55] R. McWeeny and B. T. Sutcliffe, *Methods of Molecular Quantum Mechanics* (Academic Press, London, 1969).